Quantification of microRNA editing using two-tailed RT-qPCR for improved biomarker discovery

GJENDINE VOSS,[1] ANDERS EDSJÖ,[2] ANDERS BJARTELL,[3] and YVONNE CEDER[1]

[1]Department of Laboratory Medicine, Division of Translational Cancer Research, Lund University, 22381 Lund, Sweden
[2]Department of Clinical Genetics and Pathology, Laboratory Medicine, Medical Services, Region Skåne, 22185 Lund, Sweden
[3]Department of Urology, Skåne University Hospital, 20502 Malmö, Sweden

ABSTRACT

Even though microRNAs have been viewed as promising biomarkers for years, their clinical implementation is still lagging far behind. This is in part due to the lack of RT-qPCR technologies that can differentiate between microRNA isoforms. For example, A-to-I editing of microRNAs through adenosine deaminase acting on RNA (ADAR) enzymes can affect their expression levels and functional roles, but editing isoform-specific assays are not commercially available. Here, we describe RT-qPCR assays that are specific for editing isoforms, using microRNA-379 (miR-379) as a model. The assays are based on two-tailed RT-qPCR, and we show them to be compatible both with SYBR Green and hydrolysis-based chemistries, as well as with both qPCR and digital PCR. The assays could readily detect different miR-379 editing isoforms in various human tissues as well as changes of editing levels in ADAR-overexpressing cell lines. We found that the miR-379 editing frequency was higher in prostate cancer samples compared to benign prostatic hyperplasia samples. Furthermore, decreased expression of unedited miR-379, but not edited miR-379, was associated with treatment resistance, metastasis, and shorter overall survival. Taken together, this study presents the first RT-qPCR assays that were demonstrated to distinguish A-to-I-edited microRNAs, and shows that they can be useful in the identification of biomarkers that previously have been masked by other isoforms.

Keywords: microRNAs; RT-qPCR; A-to-I editing; RNA editing; microRNA-379; prostate cancer

INTRODUCTION

Ever since their discovery in 1993 (Lee et al. 1993; Wightman et al. 1993), microRNAs (miRNAs) have been a topic of interest in both basic research and in various disease contexts. These small non-coding RNAs act through binding different mRNA targets based on imperfect sequence complementarity, and regulate both mRNA stability and translation (Pasquinelli 2012). Typically, one miRNA has hundreds of different targets in a cell, which it binds with varying affinity. This allows miRNAs to regulate several players in the same pathway and multiple biological processes at once. As such, miRNAs are thought to be crucial for the maintenance of homeostasis in a cell. It is therefore not surprising that the deregulation of miRNAs is associated with several disease states (Fabris et al. 2016; Wendt et al. 2018; Fasolo et al. 2019; van den Berg et al. 2020), which has sparked interest in their suitability both as therapeutic targets or agents and as biomarkers. The use of miRNAs as biomarkers is supported by their remarkable stability in biological fluids (Mitchell et al. 2008) and even in harshly treated specimens such as formalin-fixed tissues for several years (Hui et al. 2009). However, even though there are thousands of studies describing the association between the expression of certain miRNAs and clinical parameters, there are currently no FDA-approved miRNA biomarkers, and only a few that are ready to be used in clinical practice (Bonneau et al. 2019).

One reason for this discrepancy is the ongoing discussion on how to best normalize miRNA data, which makes it difficult to find consistent results across studies. Choosing inappropriate normalization methods can produce artefacts showing a seemingly strong deregulation that is in fact due to poor normalization (Witwer and Halushka 2016).

Another possible reason for poor translatability of miRNA biomarkers is the fact that miRNAs do not exist in only one static form, but actually occur in multiple different isoforms, which can differ in stability and carry out distinct

Corresponding author: yvonne.ceder@med.lu.se
Article is online at http://www.rnajournal.org/cgi/doi/10.1261/rna.078867.121.

functions in the cell. These different isoforms are produced by post-transcriptional modifications such as addition or removal of terminal nucleotides (isomiRs) and A-to-I editing of internal bases (Ameres and Zamore 2013).

A-to-I editing is the deamination of adenosine nucleotides to form inosine, carried out by adenosine deaminase acting on RNA (ADAR) enzymes. ADARs can target virtually any double-stranded RNA, including primary miRNAs (pri-miRNAs). As inosine preferentially base-pairs with cytosine, A-to-I editing can alter the secondary structure of pri-miRNAs, leading to an inhibition of processing and maturation, which ultimately affects expression levels. If the seed sequence is altered, this can also cause the miRNA to bind a different set of mRNA targets (Kawahara et al. 2007; Shoshan et al. 2015; Nishikura 2016; Velazquez-Torres et al. 2018; Xu et al. 2019; van der Kwast et al. 2020).

Currently, the only technology to distinguish these miRNA editing isoforms is RNA sequencing, which is time-consuming, expensive, and requires high input to detect miRNAs with low expression. Additionally, library preparation can introduce bias, making it difficult to quantify relative abundance of miRNAs accurately (Witwer and Halushka 2016).

In contrast, commonly used quantitative PCR (qPCR) methods are not specific enough to distinguish individual nucleotide differences (Androvic et al. 2017). Therefore, if only one isoform is biologically relevant in certain contexts, but other isoforms of the same miRNA are detected as well, this could mask the deregulation of the clinically relevant miRNA.

For example, recent publications have demonstrated that the ratio of isomiRs differs between cell activation states (Nejad et al. 2018b; Pillman et al. 2019), and that conventional qPCR methods are often biased and may skew the results (Wu et al. 2007; Schamberger and Orbán 2014; Magee et al. 2017; Nejad et al. 2018b). They have also shown that polyadenylation-dependent RT-qPCR protocols can potentially be adaptable for accurate isomiR quantification (Nejad et al. 2018a). Another method that has made progress toward the accurate quantification of terminal isoforms is Dumbbell-PCR (Honda and Kirino 2015). Yet, these methods do not address internal A-to-I editing. A-to-I editing-sensitive qPCR protocols have been published for mRNAs (Chen et al. 2008), but they cannot be directly transferred for miRNAs, which are much shorter. For A-to-I-edited miRNAs, no commercial assays are available, and no validated methods have been published. Studies have attempted to quantify edited and unedited mature miRNAs with custom-ordered TaqMan assays (van der Kwast et al. 2018, 2020). However, they only tested the amplification efficiency of the assays using serial dilutions of a biological sample, but provided no data regarding the cross-detection between editing isoforms. No validation using synthetic oligonucleotides to investigate amplification of each isoform on its own was carried out.

Hence, there is a dire need for an extensively validated RT-qPCR setup that can be proven to reliably distinguish A-to-I-edited miRNA isoforms. If qPCR methods can be adapted and evaluated accordingly, this could potentially improve existing miRNA biomarkers, or reveal undiscovered candidates that depend on the editing status of the miRNA.

A disease that could benefit from refined biomarkers is prostate cancer (PC), which is often curable if detected early. However, more aggressive forms do exist with a rapid progression to metastatic disease, leaving no curative treatment options and ultimately resulting in the patient's death. Finding biomarkers that early on can predict which patients are likely to develop aggressive disease and will require harsh treatment is therefore highly desirable in PC.

We have previously found that PC bone metastasis may be promoted by down-regulation of microRNA-379 (miR-379; T Catela Ivkovic, H Cornella, G Voss, et al., unpubl.), a miRNA that is known to be edited by ADAR2 at nucleotide 5 of mature miR-379-5p (Kawahara et al. 2008). The position of the edited nucleotide close to the Drosha processing site and in the seed sequence leads to both a decrease in processing efficiency (Kawahara et al. 2008) and binding of a different set of mRNA targets (Xu et al. 2019). The latter suggests that miR-379 editing isoforms may have distinct biological functions, but for lack of suitable assays, it has not been possible to pinpoint whether the anti-metastatic effect of miR-379 in PC is isoform-specific. We therefore chose miR-379 as a model to develop a method for the quantification of A-to-I-edited miRNA isoforms based on the recently described highly specific two-tailed RT-qPCR assays (Androvic et al. 2017). The principle of two-tailed RT-qPCR relies on using two short hemiprobes that bind cooperatively to prime reverse transcription (RT) rather than one longer RT primer. This greatly increases the specificity, as a single nucleotide mismatch will affect a short hemiprobe more than a long primer.

The assays developed by us were highly specific for individual editing isoforms of miR-379. Using a PC cohort, we found that the miR-379 editing frequency was higher in cancer samples compared to benign samples, and that low expression of the unedited miR-379 isoform was associated with metastasis, treatment resistance and shorter overall survival. This demonstrates that isoform-specific analysis of miRNA expression may reveal more clinical information than has been possible with previously available qPCR assays.

RESULTS AND DISCUSSION

Sensitive and isoform-specific detection of A-to-I-edited miRNAs with two-tailed RT-qPCR

To test commercially available qPCR reagents for miR-379, we used TaqMan Advanced microRNA assays for miR-379 on dilutions of unedited and edited miR-379 molecules.

We expected that they would either be specific for unedited miR-379 or recognize both isoforms indiscriminately of editing status. Instead, the assays detected both isoforms, but at vastly different PCR efficiencies (109% for unedited miR-379, 73% for edited miR-379), creating a different preference for one or the other isoform depending on the concentration (Fig. 1). This makes this assay neither suitable for distinguishing editing isoforms, nor to quantify total miR-379 reliably. In addition, the tested assay required an input of 10^5 molecules of miR-379 to detect the miRNA.

In order to achieve editing isoform-specific RT and qPCR, we designed two-tailed RT primers as previously described (Androvic et al. 2017), placing the 5′ hemiprobe so that it would cover the editing site (Fig. 2A). We tested different primer design parameters to get optimal specificity and sensitivity, trying different combinations of hemiprobe length and hemiprobe placement in relation to the edited nucleotide (Supplemental Table 1). A length of 5 nt was optimal for the 3′ hemiprobe (4 nt could not efficiently prime RT; 6 nt primed RT even of the non-target isoform, resulting in lower specificity). We found that the position of the edited nucleotide in the 5′ hemiprobe did not affect the specificity much, and ultimately we selected the probe with the highest sensitivity.

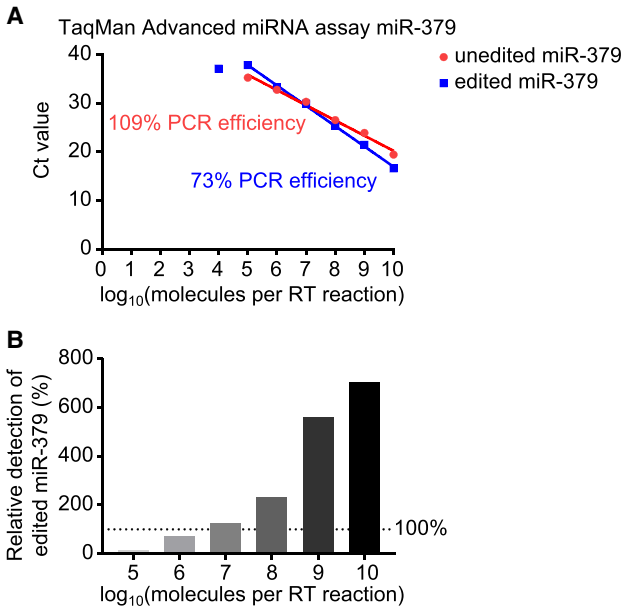

FIGURE 1. Detection of miR-379 editing isoforms with commercial TaqMan assays. (*A*) C_t values for different dilutions of unedited (red circles) and edited (blue squares) miR-379 RNA oligonucleotides quantified with TaqMan Advanced microRNA assays. PCR efficiencies were calculated based on the slope. Standard deviations were too small to be plotted as error bars. (*B*) Relative detection of edited miR-379 compared to an equal number of unedited miR-379 molecules as calculated from the difference in C_t cycles in *A*.

RT of dilutions of miR-379 RNA oligonucleotides with the two-tailed primers and subsequent SYBR Green qPCR showed that the designed probes could reliably detect their target isoforms over a large dynamic range with linearity between 100 and 10^{10} molecules per reaction (Fig. 2B) and PCR efficiencies of 85%–90%. Our RT-qPCR setting was 1000-fold more sensitive than the commercially available assay. Furthermore, the assays were very specific for their respective target isoform of miR-379 with relative detection of edited miR-379 by the unedited primers below 1%, and relative detection of unedited miR-379 by the edited primers below 0.1% (Fig. 2B). To mimic a more complex mixture of RNA molecules, the same experiments were performed with the miR-379 molecules being diluted in yeast RNA, showing largely the same result (Supplemental Fig. 1A). We also tested whether the two-tailed probes would specifically amplify only their respective target isoform in a mixture of miR-379 isoforms. The C_t value was only affected in mixtures containing 1000-fold more non-target miR-379 than target miR-379, indicating amplification of the non-target miRNA in these samples (Supplemental Fig. 1B). In all other mixtures, the C_t value remained unaffected independently of the amount of non-target miR-379 as long as target miR-379 levels remained the same.

In other contexts, it may be desirable to quantify all isoforms of a miRNA, independently of the editing status. For this purpose, we designed a pan-miR-379 RT primer with the 5′ hemiprobe shifted to bind outside of the editing site (Fig. 2C). As the reverse primers in the qPCR are designed to bind the RT-extended part of the RT primer, that is, the part that is complementary to the miRNA (Androvic et al. 2017), the reverse primers inevitably have slightly different affinities to different isoforms. We found a 60/40 mixture of edited-specific and unedited-specific reverse qPCR primers to be optimal to amplify both miR-379 isoforms equally well without bias toward one or the other isoform (Fig. 2D; Supplemental Fig. 2A). The ratio of detection of the two isoforms was close to 1.0 across all tested miR-379 concentrations, and the PCR efficiencies were 95%–100% for both isoforms, implying that amplification of miR-379 with the pan-miR-379 primers is truly independent of editing status. This was further confirmed by using miR-379 mixtures containing different ratios of the two isoforms (Supplemental Fig. 2B). The assay for pan-miR-379 amplified all different mixtures with the same C_t value, indicating isoform-blind recognition.

Finally, we wanted to ensure that in order to be able to quantify miR-379 isoforms correctly in biological samples, other closely related members of the miR-379 family (Seitz et al. 2004) would not be amplified and skew the results. The miR-379-specific RT-qPCR primers did not efficiently reverse transcribe or amplify any of the miR-379 family members, with relative detection of miR-380 below 0.001%, and no detection of miR-411 or miR-758 (Fig. 2E).

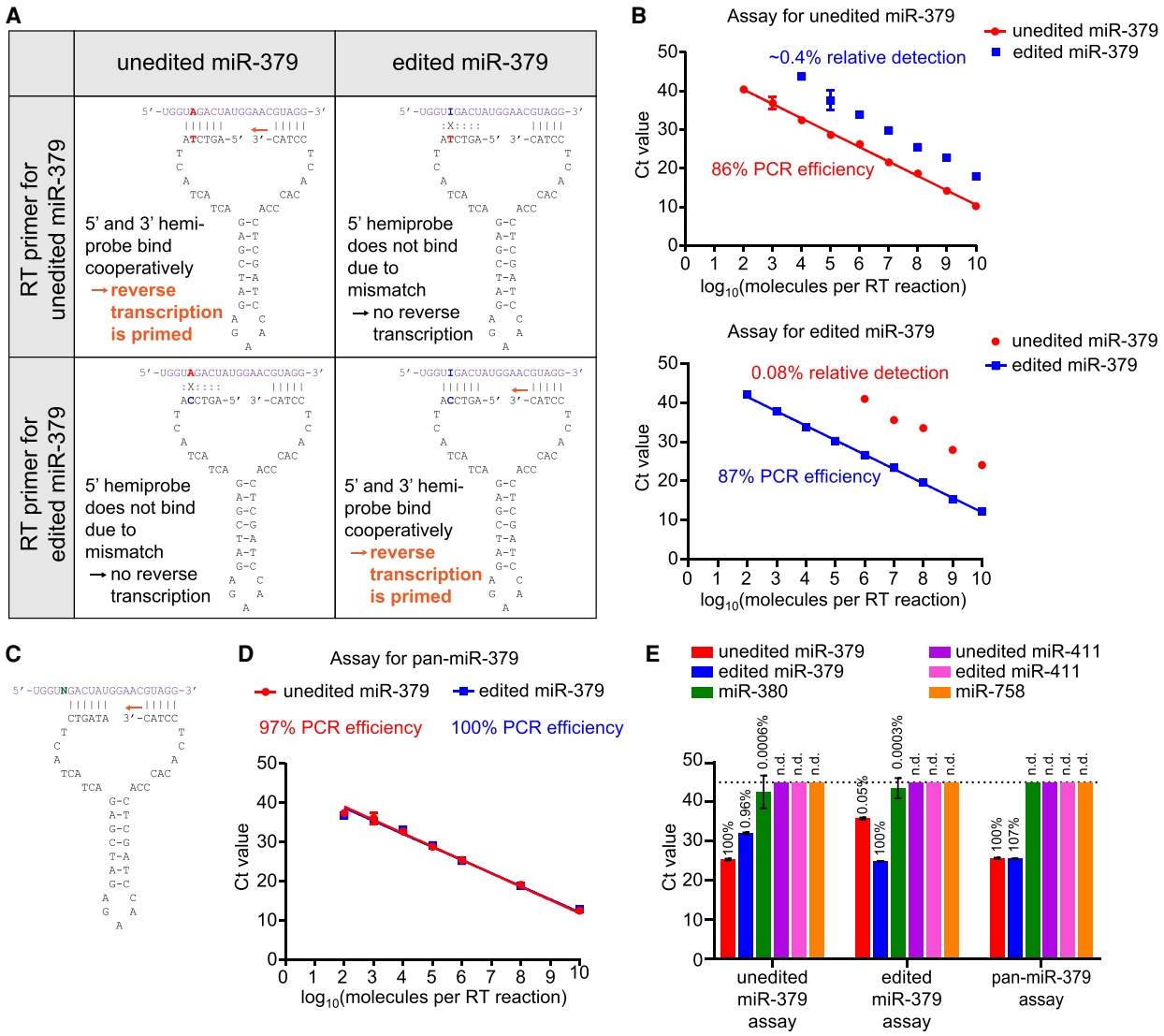

FIGURE 2. Two-tailed RT-qPCR assays for unedited, edited, or pan-miR-379. (*A*) Principle of RT primer design for editing-sensitive miR-379 assays. The 5′ hemiprobe is designed to only bind one of the two editing isoforms. Reverse transcription is only primed when both hemiprobes can bind with high affinity. (*B*) C_t values for different dilutions of unedited (red circles) and edited (blue squares) miR-379 RNA oligonucleotides quantified by the two-tailed RT-qPCR assays specific for unedited miR-379 (*top*) and edited miR-379 (*bottom*). Plots are representative of at least three independent experiments. Error bars denote the standard deviation of technical replicates; for points without error bars, the standard deviation was too small to be plotted. PCR efficiencies were calculated based on the slope. The average relative detection rate of non-target miR-379 was calculated based on the C_t difference to target miR-379. (*C*) RT primer design for the pan-miR-379 assay. The 5′ hemiprobe binds a part of the miRNA that is not subject to editing. (*D*) C_t values for different dilutions of unedited (red circles) and edited (blue squares) miR-379 RNA oligonucleotides quantified by the pan-miR-379 RT-qPCR assay. The plot is representative of at least three independent experiments. Error bars denote the standard deviation of technical replicates; for points without error bars, the standard deviation was too small to be plotted. PCR efficiencies were calculated based on the slope. (*E*) C_t values for 10^6 molecules of different miR-379 family members by the three two-tailed RT-qPCR assays. The plot is representative of two independent experiments. Error bars denote the standard deviation of technical replicates. Numbers *above* the bars indicate the relative detection of each miRNA compared to the detection of the assay's target (100%). The dotted line marks the maximum number of C_t cycles (45 cycles). Any samples that did not show amplification at a C_t lower than this are considered undetectable. (n.d.) Not detected.

Adaptation for hydrolysis probe-based qPCR and digital PCR

While SYBR Green-based two-tailed RT-qPCR is cost-efficient, there are applications for which one may want to utilize hydrolysis probes and/or digital PCR (dPCR). The distance between the forward and reverse qPCR primers allows for a 24 nt-long hydrolysis probe to be fit with a sufficiently high melting temperature and a 1–2 nt gap in between the primer and the hydrolysis probe to enable

efficient extension and qPCR. As the hydrolysis probe targets part of the 3′ hemiprobe and the stem–loop sequence of the original RT primer, that is, a sequence that is the same for both the unedited and the edited miR-379 assay, the same hydrolysis probe was used for both isoforms. Two-tailed RT-qPCR using hydrolysis probes worked well for both RT primers, with sensitivity down to 1000 molecules (Fig. 3A). However, the relative detection of the non-target miR-379 was higher than with SYBR Green, with 2% detection of edited miR-379 in the unedited miR-379-specific setting, and 0.5% detection of unedited miR-379 in the edited miR-379-specific setting. The slight decrease in both sensitivity and specificity of hydrolysis-based qPCR can potentially be outweighed by the possibility to multiplex using several fluorophores in parallel for specific applications.

Unlike qPCR, dPCR separates the PCR reaction mixture into thousands of smaller compartments, either using droplets in an emulsion, or wells on a chip. This is done at a dilution that ensures that each partition will either contain one single cDNA molecule or remain empty. After PCR, the number of positive partitions is determined (either using SYBR Green, or more commonly hydrolysis probes) and based on this, the number of cDNA molecules in the original mixture is calculated, yielding an absolute number of molecules without the need for a standard curve (Quan et al. 2018). Applying the two-tailed RT-qPCR method to chip-based dPCR showed a dynamic range up to 10^7 molecules (Supplemental Fig. 3), and satisfactory linearity with PCR efficiencies around 95%–110% (Fig. 3B,C; Supplemental Fig. 3). Once again, relative detection of the non-target miR-379 was higher than previously, with 10%–20% detection of edited miR-379 with unedited miR-379-specific primers, and 3%–15% detection of unedited miR-379 with edited miR-379-specific primers (Fig. 3B). While SYBR Green was superior to hydrolysis probes in a qPCR setting, for dPCR, SYBR Green led to a further loss of specificity with 15%–25% relative detection of edited miR-379 by unedited miR-379-specific dPCR and 7%–20% relative detection of unedited miR-379 by edited miR-379-specific dPCR (Fig. 3C). Importantly, both specificity and sensitivity of the editing-specific two-tailed assays even in the suboptimal dPCR setting were still superior to currently available commercial assays (Fig. 1).

Quantification of miR-379 editing frequency in human cells and tissues

We proceeded to test the applicability of editing-specific two-tailed RT-qPCR to quantify miR-379 editing in various

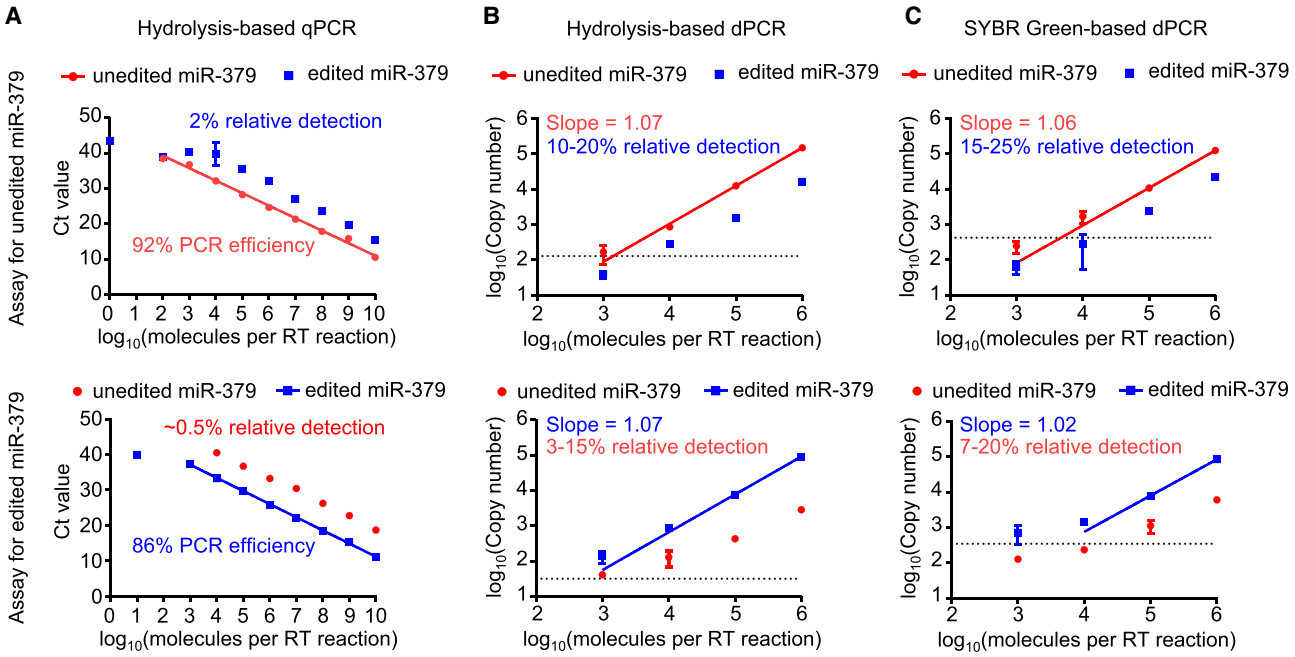

FIGURE 3. (*A*) C_t values for different dilutions of unedited (red circles) and edited (blue squares) miR-379 RNA oligonucleotides using hydrolysis probe-based qPCR for unedited (*top*) and edited (*bottom*) miR-379. Plots are representative of three independent experiments. Error bars denote the standard deviation of technical replicates; for points without error bars, the standard deviation was too small to be plotted. PCR efficiencies were calculated based on the slope. The average relative detection rate of non-target miR-379 was calculated based on the C_t difference to target miR-379. (*B*,*C*) Different dilutions of unedited (red circles) and edited (blue squares) miR-379 RNA oligonucleotides quantified by hydrolysis probe-based dPCR (*B*) and (*C*) SYBR Green-based dPCR for unedited (*top*) and edited (*bottom*) miR-379. Plots are representative of two independent experiments. Error bars denote the standard deviation of technical replicates; for points without error bars, the standard deviation was too small to be plotted. The dotted line marks the background, that is, the estimated "copy number" for negative control samples.

contexts. For this, we used SYBR Green-based qPCR, as it was the method with the highest specificity and sensitivity.

To show that our RT-qPCR can detect an increase of miR-379 editing in relevant in vitro models, we stably overexpressed different ADAR proteins (ADAR1 p110, ADAR1 p150, ADAR2) or their catalytically inactive mutants in the prostate cancer cell line PC3. ADAR overexpression was confirmed by qPCR for *ADAR* (coding for ADAR1) and *ADARB1* (coding for ADAR2) mRNA levels and by western blotting for ADAR proteins (Fig. 4A,B). We isolated RNA from the cells and quantified unedited and edited miR-379. In cells expressing either eGFP, empty vector or mutant ADAR, editing levels of mature miR-379 were very low (Fig. 4C). Upon overexpression of wild-type (WT) ADAR2, but not the mutant, there was a strong increase in miR-379 editing up to ~40% (Fig. 4C). To a much smaller extent (<10%), ADAR1 p110 and ADAR p150 were also capable of editing miR-379. We also performed total cDNA synthesis and Sanger sequencing of pri-miR-379, and could confirm widespread editing of pri-miR-379 upon ADAR2 WT overexpression, and some editing upon ADAR1 WT overexpression (Fig. 4D), supporting the findings for mature miR-379 editing.

Our findings in the ADAR-overexpressing prostate cancer cells confirm the notion that ADAR2 is the main base editor of pri-miR-379 (Kawahara et al. 2008), but also show that ADAR1 may be able to edit pri-miR-379 as well, albeit to a much smaller extent. The findings demonstrate that editing-specific two-tailed qPCR can reliably detect changes in miR-379 editing frequency.

We then tested the performance of the editing-specific RT-qPCR method on a panel of tissue RNA samples, both to demonstrate usability of the method for a broad range of tissues, and to assess the miR-379 expression levels and editing frequencies in different human tissues. All three assays (unedited miR-379, edited miR-379 and pan-miR-379) gave C_t values within the linear range of the standard curve for all tissues. Levels of miR-379 expression were highest in brain tissues and the adrenal gland (Fig. 5A; Supplemental Fig. 4A), which is in line with previous publications reporting high expression for the miR-379 cluster in the brain (Labialle et al. 2014). There was a strong correlation between levels of total miR-379 based on pan-miR-379 RT-qPCR and on the sum of unedited and edited miR-379 (Fig. 5B), indicating that the pan-miR-379 assay reliably detects both isoforms.

Editing frequencies for tissues ranged between 0.24%–11.2%, except for skin with a frequency of 0.05%. Based on the relative detection rates of the assays (Fig. 2B), any editing frequencies between 0.08%–99.6% should be correctly quantified by the assays. The detection of edited miR-379 is therefore likely not due to unspecific

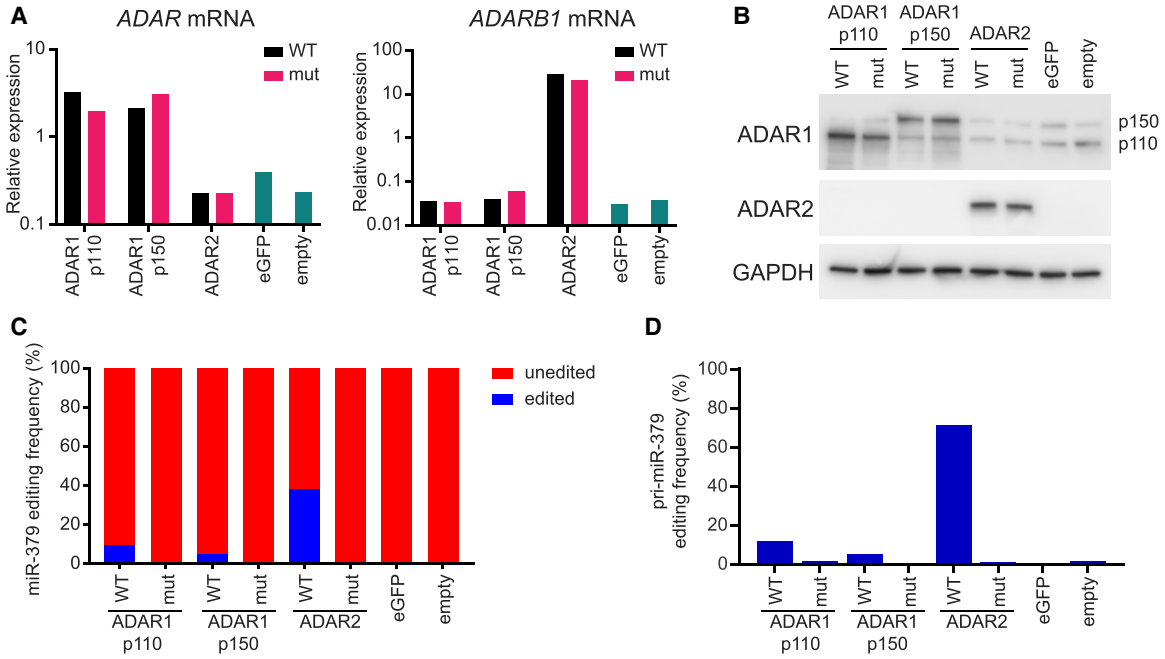

FIGURE 4. Editing of miR-379 in ADAR-overexpressing PC3 cells. (*A*) *ADAR* and *ADARB1* mRNA expression levels in PC3 cells transduced with ADAR overexpression or control vectors. Relative expression values were calculated using the geometric mean of *GUSB* and *PGK1* mRNAs for normalization. (*B*) Western blot showing ADAR1 and ADAR2 protein expression in PC3 cells transduced with ADAR overexpression or control vectors. GAPDH is the loading control. (*C*) miR-379 editing frequency in PC3 cells transduced with ADAR overexpression or control vectors. Editing frequencies were calculated based on the absolute number of edited miR-379 molecules divided by the sum of unedited and edited miR-379 molecules. Absolute numbers were derived from standard curves of serially diluted RNA oligonucleotides. (*D*) Editing frequencies of pri-miR-379 in PC3 cells transduced with ADAR overexpression or control vectors, as determined by RT-PCR and Sanger sequencing.

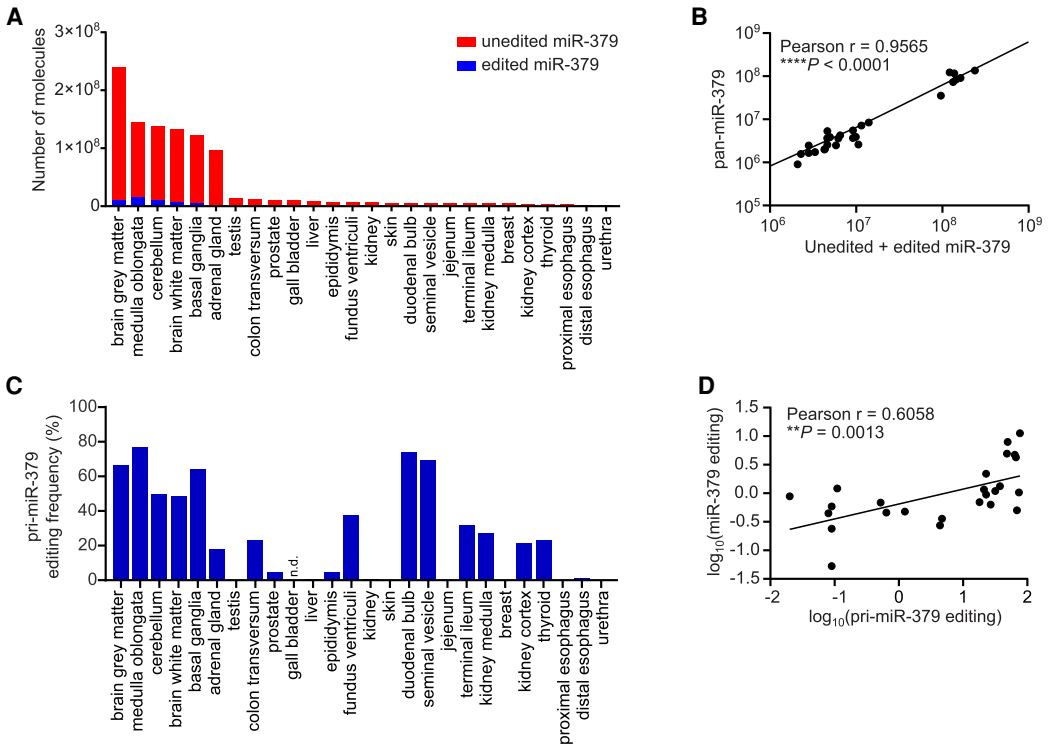

FIGURE 5. Expression and editing levels of miR-379 in a range of human tissues. (*A*) Number of molecules of unedited (red) and edited (blue) miR-379 in human tissues as determined by editing-specific two-tailed RT-qPCR. Absolute numbers were derived from standard curves of serially diluted RNA oligonucleotides, and normalized using the geometric mean of RNU24, RNU44, RNU48, and RNU66. (*B*) Correlation between the sum of unedited and edited miR-379 molecules and pan-miR-379 molecules. Absolute numbers were derived from standard curves of serially diluted RNA oligonucleotides. The *P*-value was calculated by linear regression and Pearson correlation. (*C*) Editing frequencies of pri-miR-379 in a range of human tissues as determined by RT-PCR and Sanger sequencing. From gall bladder cDNA, pri-miR-379 could not be successfully PCR-amplified. (n.d.) Not detected. (*D*) Correlation between editing frequencies of mature miR-379 and pri-miR-379 in human tissues. Variables were log-transformed to enable meaningful linear regression and Pearson correlation.

amplification of unedited miR-379 present in the sample, with the exception of the skin sample, in which edited miR-379 may not be present. The editing frequency of mature miR-379 was between 4%–12% for brain tissues (previously estimated at 15% [Kawahara et al. 2008]), around 2% for the thyroid, and around 1% or lower for all other tissues (Supplemental Fig. 4B).

Sanger sequencing of reverse-transcribed pri-miR-379 indicated higher editing frequencies across tissues (Fig. 5C), which is expected, as pri-miR-379 editing is reported to inhibit miR-379 maturation (Kawahara et al. 2008). Despite the discrepancy in magnitude, there was a statistically significant correlation between pri-miR-379 and mature miR-379 editing frequencies (Fig. 5D).

We also compared our estimates of mature miR-379 editing in tissues with published analyses of small RNA sequencing data (Skalsky and Cullen 2011; Alon et al. 2012; Warnefors et al. 2014; Pinto et al. 2017), and found that the editing frequencies in our study matched the published data well (Supplemental Fig. 5). Editing of miR-379 had been previously estimated at 4%–10% in the brain (Skalsky and Cullen 2011; Alon et al. 2012; Warnefors et al. 2014), and ranging from <1% to 3% for non-brain tissues (Warnefors et al. 2014; Pinto et al. 2017). This supports the notion that the miR-379 editing frequencies estimated by editing-sensitive two-tailed RT-qPCR correctly reflect the true editing frequencies in human tissues.

The fact that editing frequencies of both pri-miR-379 and mature miR-379 were highest in the brain is in line both with previous studies (Warnefors et al. 2014) and with reports that ADAR2 protein is mainly expressed in the brain (Melcher et al. 1996; Seitz et al. 2004). Despite this, we did not find a strong correlation between miR-379 editing frequencies and levels of *ADAR* or *ADARB1* mRNAs (Supplemental Figs. 6 and 7). This supports reports that ADAR transcript levels do not always reflect editing activity (Wahlstedt et al. 2009).

Quantification of miR-379 editing isoforms in a prostate cancer cohort

Finally, we assessed the clinical utility of our newly developed assays. We selected a clinical cohort of transurethral resections of the prostate to study miR-379 isoform regulation in PC. The cohort contained 23 tissue samples from

patients with benign prostatic hyperplasia (BPH), and 47 samples from patients with PC.

We were able to detect both unedited and edited miR-379 in all samples (Supplemental Fig. 8A), and the sum of the two isoforms correlated very well with the pan-miR-379 levels (Supplemental Fig. 9). Editing frequencies were in the range of 0.77%–52%, which is well within the previously defined reliable range of 0.08%–99.6%. There were no significant differences in relative expression comparing BPH to PC samples with any of the three assays alone (Supplemental Fig. 8A). However, the editing frequency of miR-379 was significantly higher in PC samples than BPH samples (Fig. 6A). This indicates that quantifying both editing isoforms separately can reveal clinical information that cannot be detected by any single assay.

We then focused on the PC patients and compared the association of the expression of different miR-379 isoforms with certain clinical and pathological parameters. No clear expression differences of any miR-379 isoform were observed regarding tumor stage or histological grade (Supplemental Fig. 8B,C). However, relative expression of unedited miR-379 was significantly lower in patients that already had or later developed metastases, whereas there were no statistically significant differences for edited miR-379 or pan-miR-379 (Fig. 6B). This indicates that the predictive value of miR-379 only becomes apparent when performing isoform-specific quantification, and that edited miR-379 can be a confounding factor that masks deregulation when performing isoform-blind measurements. It is likely that other isoform-specific miRNA deregulation events with clinical potential have gone unnoticed due to the lack of suitable qPCR assays.

Furthermore, patients with castration-resistant disease following hormone deprivation treatment had significantly

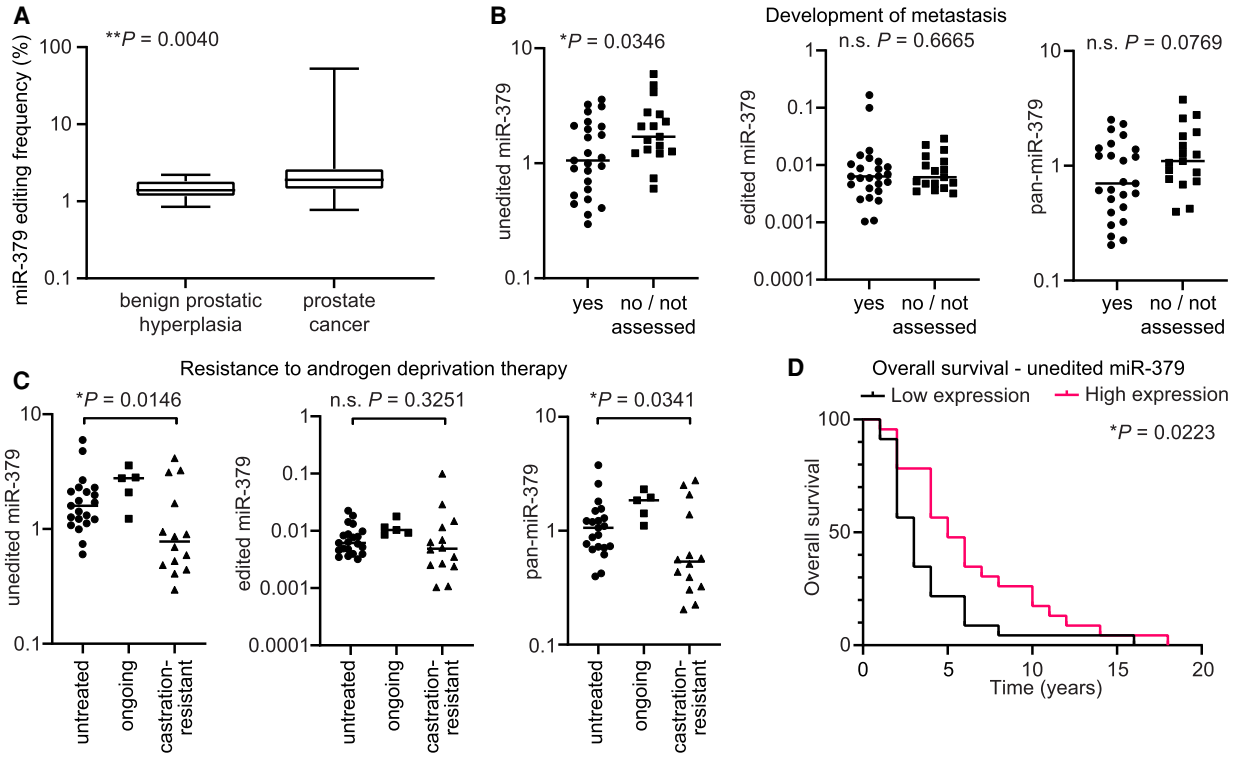

FIGURE 6. Deregulation of miR-379 editing and specific miR-379 isoforms in a prostate cancer cohort. (*A*) Editing frequency of miR-379 in 23 BPH and 47 PC patients. Editing frequencies were calculated based on the absolute number of edited miR-379 molecules divided by the sum of unedited and edited miR-379 molecules. Absolute numbers were derived from standard curves of serially diluted RNA oligonucleotides. Box plot marks the median and upper and lower quartiles, whiskers denote the range of values. Exact *P*-value was calculated using Mann-Whitney *U*-test. (*B*) Comparison of relative expression of unedited miR-379 (*left*), edited miR-379 (*middle*), and pan-miR-379 (*right*) in PC patients that developed metastasis ($n = 25$) and those that did not get metastases or in which metastasis was not suspected and therefore not assessed ($n = 17$). Expression was normalized to the geometric mean of U47, RNU48, and RNU66. Individual values and the median are shown. Exact *P*-values were calculated using Mann-Whitney *U*-tests. (n.s.) Not significant. (*C*) Comparison of relative expression of unedited miR-379 (*left*), edited miR-379 (*middle*), and pan-miR-379 (*right*) in hormone-naïve PC patients ($n = 21$), those that were currently undergoing hormone treatment ($n = 5$), and those with castration-resistant PC ($n = 14$). Expression was normalized to the geometric mean of U47, RNU48, and RNU66. Individual values and the median are shown. Exact *P*-values were calculated using Mann-Whitney *U*-tests. (n.s.) Not significant. (*D*) Survival analysis of patients with high or low relative expression of unedited miR-379. Patients were sorted by unedited miR-379 expression and divided into two groups at the median ($n = 23$ in each group). The *P*-value was calculated using log-rank test.

lower expression of unedited miR-379 and pan-miR-379, but not edited miR-379 (Fig. 6C). We also performed survival analysis and found that patients with low levels of unedited miR-379 had significantly shorter overall survival than patients with high levels (Fig. 6D). The same was observed for pan-miR-379, but not edited miR-379 (Supplemental Fig. 8D). Unlike the comparison between BPH and PC, none of the comparisons within the PC patient group showed significant differences in miR-379 editing frequency (Supplemental Fig. 10).

The fact that only unedited miR-379 was deregulated upon PC progression could suggest a potential role for this isoform in the suppression of castration resistance and metastasis, whereas edited miR-379 may not have the same role. A recent publication proposed opposite roles for unedited and edited miR-379 in multiple cancers (Xu et al. 2019). This study found unedited miR-379 to have a tumor-promoting role, whereas edited miR-379 inhibited cancer cell proliferation. However, the authors did not show any in vitro nor in vivo studies on PC cell lines, so that the role of miR-379 and its isoforms may be different in PC. This possibility is supported by a large-scale bioinformatic analysis of the TCGA data set, which found that while miR-379 editing was reduced in most tumors compared to normal tissues, it was increased in prostate tumors compared to normal tissue (Pinto et al. 2017). This matches findings in other publications that expression of *ADARB1* mRNA is up-regulated in PC, but down-regulated in many other cancer types (Paz-Yaacov et al. 2015). These in silico studies support our findings of increased miR-379 editing in PC compared to BPH.

A limitation of our study lies in the rather small size of the analyzed patient cohort, so it will be important to confirm our findings on similar cohorts in future studies. If it does hold true that unedited miR-379 is the only isoform associated with PC progression, and there is no evidence for a direct role of edited miR-379, the increase in miR-379 editing frequency in PC compared to BPH could serve as a mechanism to down-regulate unedited miR-379 expression. Editing of pri-miR-379 inhibits the maturation of miR-379 (Kawahara et al. 2008), which is supported by the finding that miR-379 editing frequency was negatively correlated with total miR-379 expression in the analyzed patient cohort (Supplemental Fig. 11).

Of course, the discussed potential functional roles of the two miR-379 isoforms are mostly speculative at this point, and would need to be confirmed mechanistically in future studies. It is also possible that, rather than a driver event in tumor progression itself, the increased miR-379 editing frequency in PC is merely a consequence of increased ADAR2 activity. This does however not limit its potential use as a biomarker. Even if there is no functional role for miR-379 editing in PC, as long as ADAR2 activity is linked to relevant clinical parameters (Shaikhibrahim et al. 2013; Paz-Yaacov et al. 2015), a panel of editing-sensitive miRNA biomarkers such as miR-379 can be an easily accessible proxy for editing activity in the tumor. Using miRNA biomarkers as an indicator of editing activity can also be interesting for other diseases in which A-to-I editing has been shown to play a role, such as glioma (Maas et al. 2001), diabetes (Gan et al. 2006), amyotrophic lateral sclerosis (Hideyama et al. 2012), and chronic viral infections (Bass et al. 1989; Weiden et al. 2014).

The principle of selecting one hemiprobe to either cover the edited nucleotide (for editing-specific assays) or a non-editable part of the miRNA (for pan-miRNA analysis) should be applicable to all miRNAs, and thereby to virtually any disease in which miRNA biomarkers have clinical potential. If the edited nucleotide is in the very middle of the miRNA sequence, there may be less room to find an optimal placement of the probe. However, given an average miRNA length of ~22 nt and the fact that only ~11 nt are covered by the hemiprobes, one should be able to place one hemiprobe over the edited nucleotide and the other in a constant region, still leaving a gap for primer extension to occur in the RT reaction. In addition, miRNA editing events are most common in nt 2–7 of the miRNA (Pinto et al. 2017). From a biological perspective, these edits in the seed sequence are also the most likely to have a strong effect on miRNA function by selecting a different target pool. Most biologically relevant miRNA editing events are therefore likely to be found in the 5′ part of the miRNA which we have shown to be easily targeted by our technology. The only real limitation lies in the fact that it may be a challenge to design pan-miRNA assays for miRNAs with more than one editing site, especially if these editing sites occur spread out over the entire length of the microRNA.

In conclusion, we here describe the first validated qPCR technology that is able to distinguish A-to-I editing isoforms of an individual miRNA. The versatility of the described assays lies not only in their compatibility with different chemistries, but also in the ease with which the primers can be adapted to different sequences. Overall, we believe that the development of A-to-I editing-specific RT-qPCR miRNA assays will serve as a useful tool for basic and translational research of miRNA function, and help develop better miRNA biomarkers for a range of diseases.

MATERIALS AND METHODS

RNA and DNA oligonucleotides

RNA oligonucleotides of unedited miR-379, edited miR-379, miR-380, unedited miR-411, edited miR-411, and miR-758 were purchased from Integrated DNA Technologies, dissolved in IDTE buffer, pH 7.5 (Integrated DNA Technologies), and then diluted in 10-fold dilution series for RT-qPCR. For experiments with yeast RNA background, 100 ng total yeast RNA (#AM7118, Invitrogen, Thermo Scientific) was added during RT sample preparation. DNA oligonucleotides were purchased from Invitrogen. Two-

tailed RT primers were designed based on a hairpin sequence published by Androvic et al. (2017) with hemiprobes designed to bind unedited or edited miR-379, and primer arms optimized to prevent the formation of unwanted secondary structures. Secondary structures of RT primers as well as secondary structures and dimers for qPCR primers were calculated using the OligoAnalyzer tool (Integrated DNA Technologies). ZEN/Iowa Black FQ double-quenched FAM-coupled miR-379 hydrolysis probe was designed using the PrimerQuest tool (Integrated DNA Technologies) and purchased from Integrated DNA Technologies. Primers for pri-miR-379 RT-PCR were based on those published by Kawahara et al. (2008), and primers for cloning were designed using the NEBuilder tool (New England Biolabs). All RNA and DNA oligonucleotide sequences are listed in Supplemental Tables 2 and 3.

Tissue and patient cohorts

The isolation of RNA from 26 human tissues was described previously (Lundwall et al. 2002). All tissues used in this study were obtained from patients undergoing surgery for neoplastic disease, or from autopsies.

Samples were collected from patients with voiding problems undergoing transurethral resection of the prostate (TURP) at Malmö University Hospital in 1990–1999. Small RNA isolation from formalin-fixed paraffin-embedded tissue sections with the mirVana miRNA Isolation Kit (Ambion) using a modified procedure was previously described (Hagman et al. 2010). In this study, 23 patients with BPH and 47 patients with PC were included. The clinical characteristics of the cohort are summarized in Supplemental Table 4.

Ethical approval for the patient cohort was obtained from the Regional Ethical Review Board in Lund, and we adhered to the Helsinki declaration for all work with human tissues.

Two-tailed RT-qPCR

For two-tailed RT-qPCR of miR-379, samples were reverse transcribed with the qScript Flex Kit (#95049-100, Quantabio) using 2 µL 5× reaction mix, 1 µL GSP enhancer, 0.05 µM two-tailed RT primer, and 0.5 µL reverse transcriptase in a total volume of 10 µL. RT was performed at 25°C for 1 h, stopped at 85°C for 5 min, and samples held at 4°C. RT products were used for qPCR or dPCR immediately. The input for RT was 2 µg RNA for cell line samples, 1 µg RNA for the human tissue panel, and 25 ng for patient samples.

The qPCR was performed with PowerUp SYBR Green Master Mix (#A25742, Thermo Scientific) using 400 nM forward and reverse primers (Supplemental Table 3). The RT product constituted up to 1/10th of the total qPCR reaction volume. Samples were assayed in triplicates using the QuantStudio 7 Flex qPCR machine (Applied Biosystems). The qPCR program consisted of 30 sec initial denaturation at 95°C, followed by 45 cycles of 5 sec at 95°C and 20 sec at 60°C. Melt curve analysis was performed to exclude the amplification of unspecific products. Absolute numbers of molecules for calculation of editing frequencies were interpolated from the C_t values by use of standard curves based on 10-fold dilutions of synthetic miR-379 oligonucleotides. For relative expression, the ΔC_t method was used to normalize miR-379 C_t values to housekeeping small RNAs (see below).

For hydrolysis-based detection of miR-379 amplification, PrimeTime Gene Expression Master Mix (#1055772, Integrated DNA Technologies) was used with 400 nM primers and a 250 nM hydrolysis probe. qPCR was performed in triplicates using a QuantStudio 7 Flex qPCR machine with initial denaturation at 95°C for 3 min, followed by 45 cycles of 5 sec at 95°C and 30 sec at 60°C.

Two-tailed RT-dPCR

Digital PCR (dPCR) was carried out using QuantStudio 3D Digital PCR Master Mix v2 (Applied Biosystems), 400 nM primers, 1 µL cDNA per reaction, and either 250 nM hydrolysis probe or 2× SYBR Green I (Life Technologies). A volume of 14.5 µL reaction mix was loaded onto QuantStudio 3D Digital PCR 20K chips v2 (Applied Biosystems) in duplicates. Amplification was carried out with initial denaturation at 96°C for 10 min, and a total of 40 cycles of 2 min at 60°C alternated with 30 sec intervals at 98°C. The chips were scanned on a QuantStudio 3D Digital PCR System (Applied Biosystems). Using QuantStudio 3D AnalysisSuite Cloud Software (Thermo Scientific), a threshold separating positive from negative wells was selected manually and applied to all chips to determine absolute copy numbers for each sample.

RT-qPCR using commercial TaqMan assays

RT with the TaqMan Advanced microRNA Kit (#A28007, Applied Biosystems) was performed according to the manufacturer's instructions. Briefly, the procedure consisted of adding a poly(A) tail and an adapter to the RNA, followed by RT using a universal RT primer and preamplification over 14 cycles. qPCR was then performed in quadruplicates using a TaqMan Advanced microRNA assay for miR-379 (#478077_mir) and TaqMan Fast Advanced Master Mix (#4444557, Applied Biosystems) according to the manufacturer's instructions on a QuantStudio 7 Flex machine.

For RT-qPCR of small RNA housekeeping controls, TaqMan microRNA assays (Applied Biosystems) were used according to the manufacturer's instructions on 100 ng (cell line samples, human tissue panel) or 1 ng (patient cohort samples) of RNA in quadruplicates. For cell line samples, the geometric mean of RNU44 (#001094) and RNU48 (#001006) was used for normalization. For the human tissue panel, the geometric mean of RNU24 (#001001), RNU44, RNU48, and RNU66 (#001002) was used for normalization. For the patient cohort, the geometric mean of U47 (#001223), RNU48 and RNU66 was used for normalization. These combinations of housekeeping genes have previously been identified as optimal for these sample sets (Larne et al. 2013).

Total cDNA synthesis

To prepare samples for pri-miR-379 and gene expression analysis, 2 µg total RNA was treated with DNase I (Thermo Scientific) according to the manufacturer's instructions at 37°C for 30 min. Total cDNA was synthesized with the High Capacity cDNA Reverse Transcription Kit (#43688114, Thermo Scientific)

according to the manufacturer's instructions using 3 µg of cell line RNA or with the RevertAid H Minus First Strand cDNA Synthesis Kit (#K1632, Thermo Scientific) according to the manufacturer's instructions using 2 µg of tissue RNA.

Gene expression analysis

For gene expression analysis, cDNA was diluted 1:5 and 1 µL of the diluted cDNA was used for qPCR using TaqMan Gene Expression assays and TaqMan Gene Expression Master Mix (#4369016, Thermo Scientific) according to the manufacturer's instructions. qPCR was performed in triplicate on a QuantStudio 7 Flex machine. Expression of *ADAR* (Hs00241666_m1) and *ADARB1* (Hs00953723_m1) was normalized to the geometric mean of *GUSB* (Hs99999908_m1) and *PGK1* (Hs99999906_m1) for cell line RNA using the ΔC_t method, or the geometric mean of *GUSB*, *PGK1*, and *GAPDH* (Hs02758991_g1) for the tissue panel.

PCR and Sanger sequencing of pri-miR-379

Pri-miR-379 cDNA was amplified from 5 µL of undiluted total cDNA with 1 U Phusion Hot Start II DNA polymerase (Thermo Scientific), 1× HF buffer, 200 µM dNTPs, and 0.5 µM primers (Supplemental Table 3) in a total reaction volume of 50 µL. The reaction program consisted of 3 min initial denaturation at 98°C, followed by 35 cycles of denaturation at 98°C for 15 sec, annealing at 64.7°C for 30 sec and extension at 72°C for 30 sec. After a final extension step for 10 min at 72°C, the PCR products were held at 4°C until PCR purification using the QIAquick PCR Purification Kit (#28106, Qiagen). DNA concentrations were determined using NanoDrop 2000 (Thermo Scientific), and PCR products were sent for Sanger sequencing to Eurofins Genomics using the forward primer used for the initial amplification. From the resulting chromatograms, peak heights of the individual nucleotides at the editing site were measured using SnapGene Viewer software (GSL Biotech; available at https://www.snapgene.com) to calculate relative editing frequencies.

Cloning of lentiviral ADAR vectors

Sequences for amino-terminally FLAG-tagged and carboxyl terminally 6×His-tagged catalytically active or mutated human ADAR1 p110 (WT or E912A mut), ADAR1 p150 (WT or E912A mut), and ADAR2 (WT or E396A mut) were amplified using the primers listed in Supplemental Table 3 from mammalian expression vectors (Heale et al. 2009), which were a kind gift from Albin Widmark and the late Marie Öhman at Stockholm University. A lentiviral expression backbone containing a CMV promoter and a puromycin resistance was amplified from pLV-CMV-LoxP-DsRed-LoxP-eGFP (Addgene #65726, a gift from Jacco van Rheenen [Zomer et al. 2015]). The primers were designed to contain complementary overhangs for NEB HiFi Assembly using the NEBuilder Tool (New England Biolabs). For control vectors, the same lentiviral backbone without an insert ("empty") or retaining the already contained eGFP ("eGFP") were PCR-amplified with primer overhangs introducing a SalI restriction site. All PCR products were produced using Phusion Hot Start II DNA polymerase (Thermo Scientific), and purified using the QIAquick PCR Purification Kit (Qiagen) according to the manufacturer's instructions. For ADAR expression vectors, the fragments were assembled using NEB HiFi Assembly (New England Biolabs) for 1 h at 50°C and transformed into chemically competent Stbl3 bacteria. For control vectors, FastDigest SalI (Thermo Scientific) was used to digest the PCR products for 90 min at 37°C and then deactivated by incubation at 65°C for 15 min, before self-circularization of the control plasmids with T4 DNA Ligase (Thermo Scientific) for 1 h at 20°C. Transformed bacteria were selected on Ampicillin plates and correct construct assembly confirmed using Sanger sequencing (Eurofins Genomics). Large-scale overnight cultures were incubated at 30°C for 24 h and plasmid DNA was extracted using the NucleoBond Xtra Midiprep Kit (Macherey-Nagel).

Cell lines and lentiviral transduction

PC3 cells were purchased from the American Tissue Culture Collection and cultured in F12 medium containing 10% FBS and 1% Penicillin-Streptomycin. HEK293T cells were a gift from Christina Möller and Professor Dr. Håkan Axelson (Lund University), and were cultured in DMEM containing 10% FBS and 1% Penicillin-Streptomycin.

For lentiviral transduction, HEK293T cells were cotransfected with 16 µg lentiviral expression vector, 6.25 µg psPAX2 packaging plasmid (Addgene #12260, a gift from Didier Trono), and 4.5 µg pMD2.G envelope plasmid (Addgene #12259, a gift from Didier Trono) using calcium-phosphate transfection. Lentiviruses were collected in IMDM containing 10% FBS and 1% Penicillin-Streptomycin for 30 h. Cell debris was removed from the virus supernatant by centrifugation at 2500 rpm and using 0.45 µm syringe filters. Cells were transduced with virus supernatant with 8 µg/mL added polybrene for 48 h, after which selection with 1 µg/mL puromycin was started. Successful transduction was confirmed through visualizing eGFP fluorescence of eGFP control cells, as detected using an Axio Vert.A1 microscope (Zeiss).

Total RNA was extracted from the cells using TRIzol reagent (Ambion) according to the manufacturer's instructions, and RNA concentrations were determined using NanoDrop.

Western blotting

Transduced cells were lysed using M-PER lysis buffer with 5 mM EDTA and HALT protease inhibitor cocktail (all Thermo Scientific) and cleared by centrifugation at 14,000*g* at 4°C for 10 min. Protein concentrations were determined using Coomassie Plus Bradford reagent (Thermo Scientific) and equal amounts of protein were prepared using Laemmli buffer (Bio-Rad) with added DTT. After denaturation at 95°C for 5 min, proteins were separated on 4%–20% Mini-Protean TGX gels (Bio-Rad) and blotted onto PVDF membranes using the TransBlot Turbo Transfer system (Bio-Rad). Membranes were blocked with blocking buffer (5% milk, 5% FBS, 1% BSA, 1 M Glycine) at room temperature and probed with primary antibodies at 4°C overnight. Primary antibodies were α-ADAR1 (sc-73408, Santa Cruz Biotechnology; 1:500), α-ADAR2 (sc-73409, Santa Cruz Biotechnology; 1:1000), and α-GAPDH (MAB374, Millipore; 1:25,000). Membranes were probed with α-mouse HRP secondary antibody (P0447, DAKO, Glostrup, Denmark) for 1 h at room

temperature, and chemiluminescence was detected using Immobilon Forte Western HRP substrate (Millipore) on an Amersham Imager 600 (GE Healthcare).

Statistical analysis

GraphPad Prism 9 (GraphPad software) was used to interpolate absolute copy numbers from standard curves, and to perform all statistical analyses. PCR efficiencies were calculated from the slope of the standard curves as follows:

$$\text{Efficiency} = -1 + 10(-1/\text{slope}).$$

For association between variables, linear regression and Pearson correlation were used. If necessary, variables were log-transformed before regression and correlation analysis. For method comparison with RNA sequencing data, Bland–Altman analysis was performed. For patient cohorts, nonparametric Mann–Whitney *U*-tests were used to compare groups, and log-rank test was used for survival analysis. A significance level of $\alpha = 0.05$ was chosen for all statistical tests.

SUPPLEMENTAL MATERIAL

Supplemental material is available for this article.

ACKNOWLEDGMENTS

We are grateful to Professor Dr. Åke Lundwall for making the human tissue panel available to us. For the prostate cancer cohort, we thank Elise Nilsson for tissue handling and Dr. Olivia Larne for the RNA extraction. We are grateful to Albin Widmark for sharing the mammalian ADAR expression plasmids with us. We also thank Christina Möller and Professor Dr. Håkan Axelson for providing the HEK293T cells. We are further grateful to Margareta Persson for excellent technical assistance and Christina Papanikolaou for her help in the transduction and maintenance of the ADAR-overexpressing cell lines. This work was supported by a grant from Kungliga Fysiografiska Sällskapet i Lund (grant number 40526) awarded to G.V., and grants from Cancerfonden (grant number CAN 2017/559), Vetenskapsrådet (grant number VR-MH 2018-03125), and Prostatacancerfonden awarded to Y.C.

Author contributions: G.V. and Y.C. conceived and designed the study and wrote the manuscript. G.V. performed all experiments. A.E. and A.B. provided clinical samples and comments during the preparation of the manuscript.

Received June 15, 2021; accepted August 18, 2021.

REFERENCES

Alon S, Mor E, Vigneault F, Church GM, Locatelli F, Galeano F, Gallo A, Shomron N, Eisenberg E. 2012. Systematic identification of edited microRNAs in the human brain. *Genome Res* **22:** 1533–1540. doi:10.1101/gr.131573.111

Ameres SL, Zamore PD. 2013. Diversifying microRNA sequence and function. *Nat Rev Mol Cell Biol* **14:** 475–488. doi:10.1038/nrm3611

Androvic P, Valihrach L, Elling J, Sjoback R, Kubista M. 2017. Two-tailed RT-qPCR: a novel method for highly accurate miRNA quantification. *Nucleic Acids Res* **45:** e144. doi:10.1093/nar/gkx588

Bass BL, Weintraub H, Cattaneo R, Billeter MA. 1989. Biased hypermutation of viral RNA genomes could be due to unwinding/modification of double-stranded RNA. *Cell* **56:** 331. doi:10.1016/0092-8674(89)90234-1

Bonneau E, Neveu B, Kostantin E, Tsongalis GJ, De Guire V. 2019. How close are miRNAs from clinical practice? A perspective on the diagnostic and therapeutic market. *Ejifcc* **30:** 114–127.

Chen YC, Kao SC, Chou HC, Lin WH, Wong FH, Chow WY. 2008. A real-time PCR method for the quantitative analysis of RNA editing at specific sites. *Anal Biochem* **375:** 46–52. doi:10.1016/j.ab.2007.12.037

Fabris L, Ceder Y, Chinnaiyan AM, Jenster GW, Sorensen KD, Tomlins S, Visakorpi T, Calin GA. 2016. The potential of microRNAs as prostate cancer biomarkers. *Eur Urol* **70:** 312–322. doi:10.1016/j.eururo.2015.12.054

Fasolo F, Di Gregoli K, Maegdefessel L, Johnson JL. 2019. Non-coding RNAs in cardiovascular cell biology and atherosclerosis. *Cardiovasc Res* **115:** 1732–1756. doi:10.1093/cvr/cvz203

Gan Z, Zhao L, Yang L, Huang P, Zhao F, Li W, Liu Y. 2006. RNA editing by ADAR2 is metabolically regulated in pancreatic islets and β-cells. *J Biol Chem* **281:** 33386–33394. doi:10.1074/jbc.M604484200

Hagman Z, Larne O, Edsjo A, Bjartell A, Ehrnstrom RA, Ulmert D, Lilja H, Ceder Y. 2010. miR-34c is downregulated in prostate cancer and exerts tumor suppressive functions. *Int J Cancer* **127:** 2768–2776. doi:10.1002/ijc.25269

Heale BS, Keegan LP, McGurk L, Michlewski G, Brindle J, Stanton CM, Caceres JF, O'Connell MA. 2009. Editing independent effects of ADARs on the miRNA/siRNA pathways. *EMBO J* **28:** 3145–3156. doi:10.1038/emboj.2009.244

Hideyama T, Yamashita T, Aizawa H, Tsuji S, Kakita A, Takahashi H, Kwak S. 2012. Profound downregulation of the RNA editing enzyme ADAR2 in ALS spinal motor neurons. *Neurobiol Dis* **45:** 1121–1128. doi:10.1016/j.nbd.2011.12.033

Honda S, Kirino Y. 2015. Dumbbell-PCR: a method to quantify specific small RNA variants with a single nucleotide resolution at terminal sequences. *Nucleic Acids Res* **43:** e77. doi:10.1093/nar/gkv218

Hui ABY, Shi W, Boutros PC, Miller N, Pintilie M, Fyles T, McCready D, Wong D, Gerster K, Jurisica I, et al. 2009. Robust global micro-RNA profiling with formalin-fixed paraffin-embedded breast cancer tissues. *Lab Invest* **89:** 597–606. doi:10.1038/labinvest.2009.12

Kawahara Y, Zinshteyn B, Sethupathy P, Iizasa H, Hatzigeorgiou AG, Nishikura K. 2007. Redirection of silencing targets by adenosine-to-inosine editing of miRNAs. *Science* **315:** 1137–1140. doi:10.1126/science.1138050

Kawahara Y, Megraw M, Kreider E, Iizasa H, Valente L, Hatzigeorgiou AG, Nishikura K. 2008. Frequency and fate of microRNA editing in human brain. *Nucleic Acids Res* **36:** 5270–5280. doi:10.1093/nar/gkn479

Labialle S, Marty V, Bortolin-Cavaillé M-L, Hoareau-Osman M, Pradère J-P, Valet P, Martin PGP, Cavaillé J. 2014. The miR-379/miR-410 cluster at the imprinted Dlk1-Dio3 domain controls neonatal metabolic adaptation. *EMBO J* **33:** 2216–2230. doi:10.15252/embj.201387038

Larne O, Martens-Uzunova E, Hagman Z, Edsjo A, Lippolis G, den Berg MS, Bjartell A, Jenster G, Ceder Y. 2013. miQ—a novel microRNA based diagnostic and prognostic tool for prostate cancer. *Int J Cancer* **132:** 2867–2875. doi:10.1002/ijc.27973

Lee RC, Feinbaum RL, Ambros V. 1993. The *C. elegans* heterochronic gene lin-4 encodes small RNAs with antisense complementarity to lin-14. *Cell* **75:** 843–854. doi:10.1016/0092-8674(93)90529-Y

Lundwall Å, Bjartell A, Olsson AY, Malm J. 2002. Semenogelin I and II, the predominant human seminal plasma proteins, are also expressed in non-genital tissues. *Mol Hum Reprod* **8:** 805–810. doi:10.1093/molehr/8.9.805

Maas S, Patt S, Schrey M, Rich A. 2001. Underediting of glutamate receptor GluR-B mRNA in malignant gliomas. *Proc Natl Acad Sci* **98:** 14687–14692. doi:10.1073/pnas.251531398

Magee R, Telonis AG, Cherlin T, Rigoutsos I, Londin E. 2017. Assessment of isomiR discrimination using commercial qPCR methods. *Non Coding RNA* **3:** 18. doi:10.3390/ncrna3020018

Melcher T, Maas S, Herb A, Sprengel R, Seeburg PH, Higuchi M. 1996. A mammalian RNA editing enzyme. *Nature* **379:** 460–464. doi:10.1038/379460a0

Mitchell PS, Parkin RK, Kroh EM, Fritz BR, Wyman SK, Pogosova-Agadjanyan EL, Peterson A, Noteboom J, Briant KC, Allen A, et al. 2008. Circulating microRNAs as stable blood-based markers for cancer detection. *Proc Natl Acad Sci* **105:** 10513. doi:10.1073/pnas.0804549105

Nejad C, Pépin G, Behlke MA, Gantier MP. 2018a. Modified polyadenylation-based RT-qPCR increases selectivity of amplification of 3′-microRNA isoforms. *Front Genet* **9:** 11. doi:10.3389/fgene.2018.00011

Nejad C, Pillman KA, Siddle KJ, Pépin G, Änkö M-L, McCoy CE, Beilharz TH, Quintana-Murci L, Goodall GJ, Bracken CP, et al. 2018b. miR-222 isoforms are differentially regulated by type-I interferon. *RNA* **24:** 332–341. doi:10.1261/rna.064550.117

Nishikura K. 2016. A-to-I editing of coding and non-coding RNAs by ADARs. *Nat Rev Mol Cell Biol* **17:** 83–96. doi:10.1038/nrm.2015.4

Pasquinelli AE. 2012. MicroRNAs and their targets: recognition, regulation and an emerging reciprocal relationship. *Nat Rev Genet* **13:** 271–282. doi:10.1038/nrg3162

Paz-Yaacov N, Bazak L, Buchumenski I, Porath HT, Danan-Gotthold M, Knisbacher BA, Eisenberg E, Levanon EY. 2015. Elevated RNA editing activity is a major contributor to transcriptomic diversity in tumors. *Cell Rep* **13:** 267–276. doi:10.1016/j.celrep.2015.08.080

Pillman KA, Goodall GJ, Bracken CP, Gantier MP. 2019. miRNA length variation during macrophage stimulation confounds the interpretation of results: implications for miRNA quantification by RT-qPCR. *RNA* **25:** 232–238. doi:10.1261/rna.069047.118

Pinto Y, Buchumenski I, Levanon EY, Eisenberg E. 2017. Human cancer tissues exhibit reduced A-to-I editing of miRNAs coupled with elevated editing of their targets. *Nucleic Acids Res* **46:** 71–82. doi:10.1093/nar/gkx1176

Quan P-L, Sauzade M, Brouzes E. 2018. dPCR: a technology review. *Sensors (Basel)* **18:** 1271. doi:10.3390/s18041271

Schamberger A, Orbán TI. 2014. 3′ IsomiR species and DNA contamination influence reliable quantification of microRNAs by stem-loop quantitative PCR. *PLoS One* **9:** e106315. doi:10.1371/journal.pone.0106315

Seitz H, Royo H, Bortolin ML, Lin SP, Ferguson-Smith AC, Cavaillé J. 2004. A large imprinted microRNA gene cluster at the mouse Dlk1-Gtl2 domain. *Genome Res* **14:** 1741–1748. doi:10.1101/gr.2743304

Shaikhibrahim Z, Lindstrot A, Ochsenfahrt J, Fuchs K, Wernert N. 2013. Epigenetics-related genes in prostate cancer: expression profile in prostate cancer tissues, androgen-sensitive and -insensitive cell lines. *Int J Mol Med* **31:** 21–25.

Shoshan E, Mobley AK, Braeuer RR, Kamiya T, Huang L, Vasquez ME, Salameh A, Lee HJ, Kim SJ, Ivan C, et al. 2015. Reduced adenosine-to-inosine miR-455-5p editing promotes melanoma growth and metastasis. *Nat Cell Biol* **17:** 311–321. doi:10.1038/ncb3110

Skalsky RL, Cullen BR. 2011. Reduced expression of brain-enriched microRNAs in glioblastomas permits targeted regulation of a cell death gene. *PLoS One* **6:** e24248. doi:10.1371/journal.pone.0024248

van den Berg MMJ, Krauskopf J, Ramaekers JG, Kleinjans JCS, Prickaerts J, Briedé JJ. 2020. Circulating microRNAs as potential biomarkers for psychiatric and neurodegenerative disorders. *Prog Neurobiol* **185:** 101732. doi:10.1016/j.pneurobio.2019.101732

van der Kwast R, van Ingen E, Parma L, Peters HAB, Quax PHA, Nossent AY. 2018. Adenosine-to-inosine editing of microRNA-487b alters target gene selection after ischemia and promotes neovascularization. *Circ Res* **122:** 444–456. doi:10.1161/CIRCRESAHA.117.312345

van der Kwast RVCT, Parma L, van der Bent ML, van Ingen E, Baganha F, Peters HAB, Goossens EAC, Simons KH, Palmen M, de Vries MR, et al. 2020. Adenosine-to-inosine editing of vasoactive microRNAs alters their targetome and function in ischemia. *Mol Ther* **21:** 932–953.

Velazquez-Torres G, Shoshan E, Ivan C, Huang L, Fuentes-Mattei E, Paret H, Kim SJ, Rodriguez-Aguayo C, Xie V, Brooks D, et al. 2018. A-to-I miR-378a-3p editing can prevent melanoma progression via regulation of PARVA expression. *Nat Commun* **9:** 461. doi:10.1038/s41467-018-02851-7

Wahlstedt H, Daniel C, Enstërö M, Öhman M. 2009. Large-scale mRNA sequencing determines global regulation of RNA editing during brain development. *Genome Res* **19:** 978–986. doi:10.1101/gr.089409.108

Warnefors M, Liechti A, Halbert J, Valloton D, Kaessmann H. 2014. Conserved microRNA editing in mammalian evolution, development and disease. *Genome Biol* **15:** R83. doi:10.1186/gb-2014-15-6-r83

Weiden MD, Hoshino S, Levy DN, Li Y, Kumar R, Burke SA, Dawson R, Hioe CE, Borkowsky W, Rom WN, et al. 2014. Adenosine deaminase acting on RNA-1 (ADAR1) inhibits HIV-1 replication in human alveolar macrophages. *PLoS One* **9:** e108476. doi:10.1371/journal.pone.0108476

Wendt A, Esguerra JL, Eliasson L. 2018. Islet microRNAs in health and type-2 diabetes. *Curr Opin Pharmacol* **43:** 46–52. doi:10.1016/j.coph.2018.08.003

Wightman B, Ha I, Ruvkun G. 1993. Posttranscriptional regulation of the heterochronic gene lin-14 by lin-4 mediates temporal pattern formation in *C. elegans*. *Cell* **75:** 855–862. doi:10.1016/0092-8674(93)90530-4

Witwer KW, Halushka MK. 2016. Toward the promise of microRNAs: enhancing reproducibility and rigor in microRNA research. *RNA Biol* **13:** 1103–1116. doi:10.1080/15476286.2016.1236172

Wu H, Neilson JR, Kumar P, Manocha M, Shankar P, Sharp PA, Manjunath N. 2007. miRNA profiling of naïve, effector and memory CD8 T cells. *PLoS One* **2:** e1020. doi:10.1371/journal.pone.0001020

Xu X, Wang Y, Mojumdar K, Zhou Z, Jeong KJ, Mangala LS, Yu S, Tsang YH, Rodriguez-Aguayo C, Lu Y, et al. 2019. A-to-I-edited miRNA-379-5p inhibits cancer cell proliferation through CD97-induced apoptosis. *J Clin Invest* **129:** 5343–5356. doi:10.1172/JCI123396

Zomer A, Maynard C, Verweij Frederik J, Kamermans A, Schäfer R, Beerling E, Schiffelers Raymond M, de Wit E, Berenguer J, Ellenbroek Saskia Inge J, et al. 2015. *In vivo* imaging reveals extracellular vesicle-mediated phenocopying of metastatic behavior. *Cell* **161:** 1046–1057. doi:10.1016/j.cell.2015.04.042